Journal of Palaeogeography

ORIGINAL ARTICLE Open Access

Triassic (Anisian and Rhaetian) palaeomagnetic poles from the Germanic Basin (Winterswijk, the Netherlands)

Lars P. P. van Hinsbergen[1], Douwe J. J. van Hinsbergen[2*], Cor G. Langereis[2], Mark J. Dekkers[2], Bas Zanderink[2,3] and Martijn H. L. Deenen[2]

Abstract

In this paper, we provide two new Triassic palaeomagnetic poles from Winterswijk, the Netherlands, in the stable interior of the Eurasian plate. They were respectively collected from the Anisian (~ 247–242 Ma) red marly limestones of the sedimentary transition of the Buntsandstein Formation to the dark grey limestones of the basal Muschelkalk Formation, and from the Rhaetian (~ 208–201 Ma) shallow marine claystones that unconformably overlie the Muschelkalk Formation. The magnetization is carried by hematite or magnetite in the Anisian limestones, and iron sulfides and magnetite in the Rhaetian sedimentary rocks, revealing for both a large normal polarity overprint with a recent (geocentric axial dipole field) direction at the present latitude of the locality. Alternating field and thermal demagnetization occasionally reveal a stable magnetization decaying towards the origin, interpreted as the Characteristic Remanent Magnetization. Where we find a pervasive (normal polarity) overprint, we can often still determine well-defined great-circle solutions. Our interpreted palaeomagnetic poles include the great-circle solutions. The Anisian magnetic pole has declination $D \pm \Delta D_x = 210.8 \pm 3.0°$, inclination $I \pm \Delta I_x = -26.7 \pm 4.9°$, with a latitude, longitude of 45.0°, 142.0° respectively, $K = 43.9$, $A_{95} = 2.9°$, $N = 56$. The Rhaetian magnetic pole has declination $D \pm \Delta D_x = 32.0 \pm 8.7°$, inclination $I \pm \Delta I_x = 50.9 \pm 8.1°$, with a latitude, longitude of 60.6°, 123.9° respectively, $K = 19.3$, $A_{95} = 7.4°$, $N = 21$. The poles plot close to the predicted location of global apparent polar wander paths (GAPWaPs) in Eurasian coordinates and are feasible for future apparent polar wander path construction. They confirm that the intracontinental, shallow-marine Germanic Basin, in which the Muschelkalk Formation was deposited, existed at a palaeolatitude of 14.1° [11.3, 17.1] N, in a palaeo-environment reminding of the Persian Gulf today. In Rhaetian times, palaeolatitudes of 31.6° [24.8, 39.8] N were reached, on its way to the modern latitude of 52°N.

Keywords: Palaeomagnetic, Palaeolatitude, Anisian, Rhaetian, Muschelkalk Formation, Germanic Basin

1 Introduction

Palaeogeographic reconstructions provide essential context and boundary conditions for the study of deep-time geological, climatological, and biological processes (Blakey 2008; Scotese and Schettino 2017; Torsvik and Cocks 2017). For times of the supercontinent Pangea, in Triassic time (~ 251–201 Ma), such reconstructions are primarily based on plate tectonic reconstructions using marine magnetic anomalies, which show how continents and oceans have moved relative to each other (e.g., Seton et al. 2012). Subsequently, plate margins are corrected for intense plate boundary zone deformation using structural geological constraints (e.g., Hall 2002; Boschman et al. 2014; van Hinsbergen et al. 2014, 2019). To these reconstructions, geographical features such as coastlines, mountain belts, lakes and seas, and icecaps are then added using geological data (Vérard et al. 2015; Baatsen et al. 2016; Scotese and Schettino 2017; Torsvik and Cocks 2017). Finally, to use the reconstruction as basis for wider geoscientific study, the reconstruction needs to be placed in a reference frame that determines the position of the plates, continents, and oceans relative

* Correspondence: D.j.j.vanhinsbergen@uu.nl
[2]Department of Earth Sciences, Utrecht University, Princetonlaan 8A, 3584 CB Utrecht, the Netherlands
Full list of author information is available at the end of the article

to the Earth's spin axis (for palaeo-climate and environment studies), or relative to modern mantle structure (for studies on geodynamic processes) (e.g., Cox and Hart 1986; Besse and Courtillot 2002; Torsvik et al. 2008; Kent and Irving 2010; van Hinsbergen et al. 2015).

On geological timescales, the Earth's magnetic field may be described as dipolar, aligning along the spin axis (e.g., Tauxe 2010). The positions of plates relative to the poles are then reconstructed by measuring the palaeomagnetic field recorded by and preserved in rocks. From the direction of the magnetic field preserved in a rock, a location may be calculated of the associated palaeomagnetic pole, and when that pole does not coincide with the modern geographic north pole, net plate motion relative to such poles may be calculated (e.g., Tauxe 2010). With relative motions of major plates relative to each other constrained, all poles from stable plate interiors may be rotated into a common reference location, and a global apparent polar wander path (GAPWaP) may be calculated (e.g., Besse and Courtillot 2002; Kent and Irving 2010; Torsvik et al. 2012). A GAPWaP provides the position of a palaeogeographic reconstruction of plates and continents relative to the Earth's spin axis, and forms the reference for studies applying palaeomagnetism to reconstruct intensely deformed plate boundary zones, or to reconstruct plates from intensely deformed relics accreted at plate boundaries (e.g., Nokleberg et al. 2000). Whereas applications of the available GAPWaP are numerous, and palaeomagnetic datasets aiming to constrain regional deformation relative to major plates rapidly increase in size (e.g., Cogné et al. 2013; Li et al. 2017), new data from tectonically quiet plate interiors are sparse, and the resolution of the reference GAPWaP may become a limiting factor (Dupont-Nivet et al. 2010). It is therefore important to collect new poles from stable continental interiors.

In this paper, we provide such a new pole, from the Netherlands. During the Anisian, the area of the Netherlands was located in the Germanic Basin in the heart of Pangea (Ziegler 1992). During the Early Triassic, a regional transgression drowned a widespread fluviolacustrine basin (Buntsandstein), to give way to the deposition of a shallow-marine carbonate formation known as the Muschelkalk Formation (e.g., Ziegler 1992). Deformation in the region was restricted to some normal faulting, and palaeomagnetic poles from Northwest Europe are widely considered representative for stable Eurasia (e.g., Torsvik et al. 2012). In the Netherlands, the Buntsandstein-Muschelkalk sedimentary environment transition is exposed in the quarries of Winterswijk (Fig. 1), and is dated as the Anisian (Herngreen et al. 2005) (Middle Triassic, 247.2–242 Ma; Gradstein et al. 2012). Here we report palaeomagnetic and rock magnetic analyses of rocks from red and white marly limestones and carbonates from the Anisian uppermost Buntsandstein Formation and lowermost Muschelkalk, and from overlying Rhaetian dark grey claystones, to constrain new palaeomagnetic poles, and provide a first-order reconstruction displaying the position of the Winterswijk deposits in their palaeogeographic context.

2 Geological setting and sampling

The 'Winterswijksche Steen- en Kalkgroeve' (51.97°N, 6.78°E) comprises a series of quarries near Winterswijk, in the east of the Netherlands (Fig. 1), where the lower Muschelkalk Formation is mined for building material. The base of the quarry exposes a ~ 3°-9° dipping monoclinal succession, consisting of ~ 40 m thick section comprising the top few meters of Buntsandstein red marly limestone, followed by a transition of paralic Muschelkalk blue-grey marly limestones to the shallow marine (Herngreen et al. 2005) (Fig. 1). This well-dated section, palynologically constrained at the Anisian (247.2–242 Ma; Herngreen et al. 2005), has a rich fossil fauna, which has been subject to numerous palaeontological studies. These recovered ichnofossils and tetrapod footprints (Oosterink 1976; Demathieu and Oosterink 1988; Diedrich 2000; Schulp et al. 2017), reptiles (nothosaurs and placodonts) (Albat 1999; Bickelmann and Sander 2008; Klein 2009, 2012; Klein and Albers 2009; Albers 2011; Klein and Scheyer 2013; Klein and Sichelschmidt 2014; Sander et al. 2014; Klein et al. 2015, 2016; Voeten et al. 2015, 2018; Maxwell et al. 2016; During et al. 2017; Klein and Griebeler 2018; Heijne et al. 2019), but also lobsters (Klompmaker and Fraaije 2011), jellyfish (Klompmaker and Fraaije 2011), and insects (van Eldijk et al. 2017). The Muschelkalk Formation contains widespread secondary mineralizations in cracks and pores, containing like pyrite and celestine (Kloprogge et al. 2001).

The Muschelkalk Formation is unconformably covered by the uppermost Triassic (Rhaetian, 208.5–201.3 Ma; Gradstein et al. 2012), pyrite-bearing, poorly consolidated claystone (Herngreen et al. 2005). Besides, subrosion pipes (sinkholes) were found within the Muschelkalk, interpreted to a result from the collapse of subsurface cavities that are thought to have formed due to the dissolution of Zechstein salts of the underlying Permian sequence (e.g., Klompmaker et al. 2010). These are filled with the Rhaetian-Hettangian (the uppermost Triassic to the lowermost Jurassic) ammonite-bearing claystone (Herngreen et al. 2005; Oosterink et al. 2006; Klompmaker and Van den Berkmortel 2007; Klompmaker et al. 2010).

We collected 222 palaeomagnetic core samples from nine stratigraphic horizons (WW 1–9) across the 40 m of the Muschelkalk Formation: 80 from four horizons of red marly limestone (WW 1, 5–7) (Fig. 1d), and 142 from grey limestone (WW 2–4, 8–9) (Fig. 1b, c). At each stratigraphic horizon, 20–40 samples were collected across an approximately 1.5 m thick interval, which with

Fig. 1 **a** - Map of Europe with location of the Winterswijk sampling site in the east of the Netherlands; **b-c** - Field photographs of the sampled Muschelkalk Formation limestones; **d** - Field photograph of the sampled red marly limestones interlayered with the Muschelkalk Formation limestones; **e** - Field photograph of the Rhaetian Formation claystones, which were so soft that they were sampled with plastic tubes, here sticking out of the sediments

typical sedimentation rates of several to tens of cm/kyr is sufficient to assume the palaeomagnetic direction scatter obtained from these horizons or from all horizons combined and represent the secular variation of the geomagnetic field. Sampling occurred with a water-cooled, generator-powered electric drill, and samples were oriented with a magnetic compass. Orientations needed no correction for the local declination (0° at the time of sampling). In addition, we collected 73 samples from a ~ 1 m thick section (WW 10) of Rhaetian claystones unconformably overlying the Muschelkalk Formation on the north side of the quarry. Because these clays were poorly consolidated and disintegrated during sampling with a water-cooled drill, we collected samples using 25 mm diameter plastic tubes that were hammered into the clays (Fig. 1e), a common sampling technique for poorly consolidated sediments (e.g., Sier et al. 2011). The benefit of the tubes was that they have the same size as regular palaeomagnetic cores and could in the field be oriented with a magnetic compass and extracted from the exposure.

3 Methods

Cores and sample tubes were cut into standard specimens of 25 mm diameter and 22 mm length. At least one specimen per core was demagnetized. We carried out the laboratory analyses at Paleomagnetic Laboratory Fort Hoofddijk, Utrecht University, the Netherlands.

The natural remanent magnetization (NRM) of at least one specimen per core or tube sample was progressively demagnetized according to standard stepwise palaeomagnetic practice (Zijderveld 1967). Thermal demagnetization was done with steps of 20–50 °C up to 680 °C using an ASC thermal demagnetizer (model TD48, residual field < 10 nT) and remaining NRMs were measured with a '2G' enterprises DC SQUID (Direct Current Superconducting Quantum Interference Device) magnetometer with a noise level of 3×10^{-12} Am^2. Alternating field (AF) demagnetization was done with steps of 5–10 mT up to 100 mT using the robotized demagnetization setup at Fort Hoofddijk (Mullender et al. 2016). The tube samples from the Rhaetian claystones were only AF demagnetized as they were contained in a plastic tube. A total of 192 specimens from cores of the Anisian red marly limestones and grey limestones of the lower Muschelkalk were AF demagnetized and an additional 48 specimens were demagnetized thermally (see Additional files 1 and 2).

Demagnetization diagrams were plotted on orthogonal vector diagrams (Zijderveld 1967), and interpreted via principal component analysis (Kirschvink 1980) as criterion for determining the linearity or planarity of demagnetization data (when a single directional component is being demagnetized forming a linear segment, or when two coercivity or blocking temperature spectra overlap forming great circles demagnetization paths) in terms of Maximum Angular Deviation (MAD) values. Mean directions for the Anisian and Rhaetian samples were calculated combining lines and converging planes based on all available data for each stratigraphic interval (McFadden and McElhinny 1988). In fitting the great circles, we determine the modified α_{95} (αm_{95}) for setpoints and great circle solutions, as given by McFadden and McElhinny (1988). Paleomagnetism.org also provides the full α_{95} as derived from their equation (25). Directional means, as well as means of the virtual geomagnetic poles (VGPs), were calculated according to Fisher (1953), including their corresponding dispersion and cones of confidence (k, α_{95} and K, A_{95}, respectively). Errors in declination (ΔD_x) and inclination (ΔI_x) were determined from A_{95} according to Butler (1992). We used the criteria of Deenen et al. (2011, 2014) to determine whether secular variation has been sufficiently sampled, based on the N-dependent envelope of A_{95} (A_{95min}-A_{95max}). A fixed cut-off (45°) was applied to remove outliers. For interpretation and statistical treatment, we used the online palaeomagnetic analysis platform Paleomagnetism.org (Koymans et al. 2016). Files compatible with this platform containing all data and interpretations are provided in the Additional files 1 and 2.

To determine the nature of the magnetic carriers, we performed rock magnetic analyses including thermomagnetic runs (5 samples) with a modified horizontal translation-type Curie balance with a cycling applied magnetic field of 150–300 mT (Mullender et al. 1993). To discriminate between thermochemical alteration during the experiment and truly magnetic behavior, we cycled to increasingly elevated temperatures with cooling segments in between, 250 °C, 150 °C, 350 °C, 250 °C, 450 °C, 350 °C, 520 °C, 420 °C, 620 °C, 500 °C, 700 °C; the entire sequence was room temperature. In addition, we measured detailed acquisition curves of the isothermal remanent magnetization (IRM) up to 700 mT (61 IRM field levels; 52 specimens) using the robotized 2G Enterprises SQUID magnetometer with in-line alternating field (AF) demagnetization and IRM acquisition facilities (Mullender et al. 2016). The latter is a laboratory-induced remanence that is used to characterize the magnetic minerals carrying the NRM along with their grain size that further serves to make inferences concerning the palaeomagnetic stability of the NRM. IRM acquisition curves were obtained from the so-called static 3-axes AF demagnetized starting state, with the final AF demagnetization axis parallel to the subsequent IRM (pulse) fields. In this way, there is a minimal deviation in the shape of the measured IRM acquisition curve from a cumulative log-Gaussian distribution (cf. Heslop et al. 2004). Thus, before the IRM acquisition, we demagnetized the samples along three orthogonal axes at 300 mT AF using a laboratory-built

demagnetization coil. IRM coercivity fraction fitting was done with the interactive software package of Kruiver et al. (2001) that assumes cumulative log-Gaussian IRM acquisition curves are linearly additive. Each coercivity fraction is determined by three parameters: SIRM (saturation IRM; the amount of the specific magnetic mineral), $B_{1/2}$ (the IRM acquisition field at which 50% of the IRM is reached) and DP (dispersion parameter, describing the width of an IRM coercivity distribution). An IRM acquisition curve is the sum of several of such coercivity components. In reality, IRM acquisition curves are often not completely log-Gaussian, which is a consequence of thermal activation, in particular, fine-grained particles close to the superparamagnetic threshold (~ 30 nm at room temperature), and show time-dependent behavior. This results in "skewed-to-the-left" coercivity distributions (Egli 2004; Heslop et al. 2004) which require an additional coercivity component for a proper fitting in the Kruiver et al. (2001) package. In the interpretation, the amount of skew-component is added to that of the soft component, representing magnetite (*sensu lato*, thus including partially oxidized magnetite, i.e., the range of compositions between Fe_3O_4 and γ-Fe_2O_3). The hard IRM component then represents hematite (α-Fe_2O_3).

4 Results

4.1 Rock magnetism

4.1.1 Thermomagnetic analysis

Thermomagnetic runs indicate that samples are only weakly magnetic as expected for these types of sediments (Fig. 2). WW 1.14 and WW 6.14 are from the Anisian red marly limestones. They are essentially paramagnetic; during cycling above 500 °C some magnetization is lost but a smaller magnetization emerges during the final cooling runs. Both samples show a minutely expressed Néel point of hematite. WW 6.14 shows some reaction to magnetite starting at ~ 430 °C; presumably, during the thermomagnetic run, pyrite is being oxidized via magnetite to hematite. WW 3.21b and WW 8.3c are from the Anisian grey limestones. They are weakly magnetic only with WW 3.21b showing no measurable ferromagnetism. In WW 8.3c the oxidation reaction of pyrite is markedly present. Apparently, both red and grey limestones have variable amounts of pyrite. The sample WW 10.61b from the Rhaetian claystone, is fully reversible to 250 °C. The small 'hump' at 300–350 °C may indicate ferrihydrite conversion to magnetite due to the reducing capacity of organic matter, which then converts to hematite at higher temperatures. The increase starting at ~ 400 °C is interpreted to be caused by pyrite oxidation, again first to magnetite and finally to hematite (e.g., Passier et al. 2001). Hematite's presence is clear from its Néel point at ~ 675 °C. Magnetite is completely oxidized to hematite at elevated temperature since a Curie point does not reappear during the final cooling run (from 700 °C to room temperature). It should be noted that the negative magnetic moment at high temperature in some samples due to diamagnetism of the quartz glass sample holder. The magnetite formation during the thermomagnetic experiment has a direct bearing on thermal demagnetization of the NRM: it does not bode well for samples that contain traces of pyrite. The impossibility to thermally demagnetize the samples because they were contained in plastic tubes, therefore, was of little influence: the spurious magnetic moment of the formed magnetite would have completely obscured the NRM

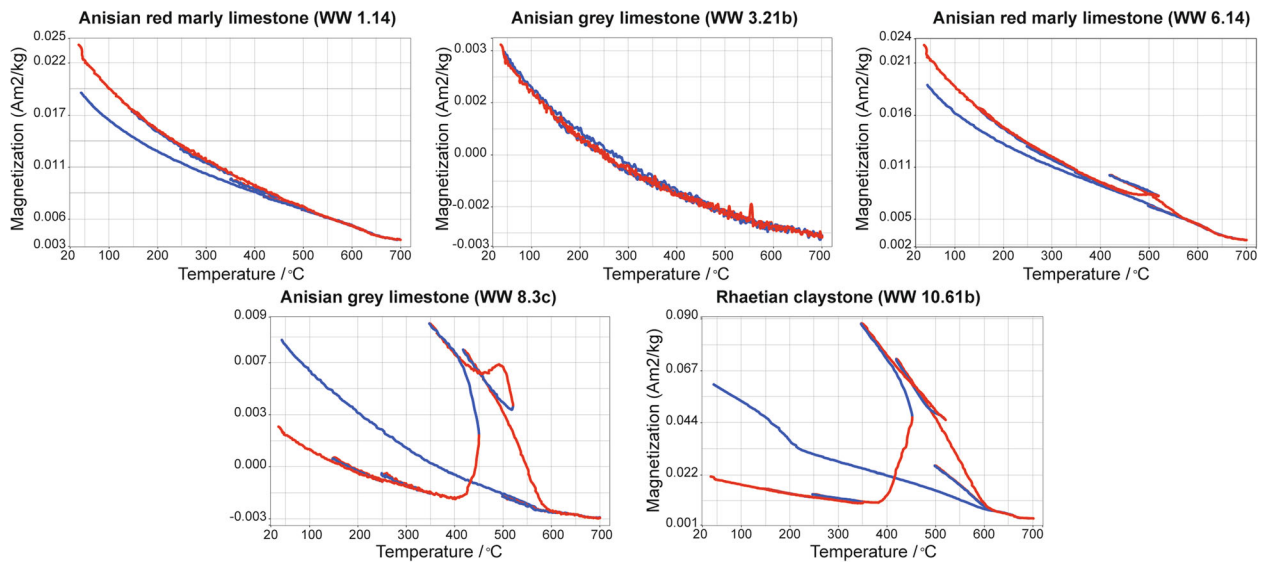

Fig. 2 Thermomagnetic runs with the modified horizontal translation Curie balance (Mullender et al. 1993). Red line represents heating segments; blue line represents intervening cooling segments and final cooling runs; temperature segments are specified in the main text

during thermal demagnetization steps above ~ 450 °C. This is why the Rhaetian samples were treated with AF demagnetization solely.

4.1.2 IRM acquisition curves

The IRM acquisition curves are fitted with three components of which two are deemed meaningful and interpreted (Additional file 1: Supplementary Information 1a). Component 1 with $B_{1/2}$ ranging from ~ 150 mT to over 1 T, typically between 250 mT and 350 mT, is interpreted as hematite. Samples with a high contribution of this component are often reddish colored. Component 2 with $B_{1/2}$ ranging from ~ 50 mT to ~ 70 mT, often in between ~ 55 mT and ~ 65 mT, is interpreted as magnetite oxidized to a variable degree. The third, lowest field, component (component 3; Additional files 1 and 2) is inferred to be the consequence of thermal activation; its amount is added to the component 2. It is inherent to the symmetric distributions in the log-Gaussian field space enforced by the fitting package. Below we illustrate the IRM acquisition behavior (Fig. 3). Sample WW 2.4B (Fig. 3) from the Anisian grey limestone has an appreciable hematite contribution (62.5% of the total (calculated) IRM). It is magnetically notably hard with a $B_{1/2}$ of ~ 760 mT; its dispersion parameter of 0.42 (all DP are in log units) is fairly high but not uncommon for an antiferromagnetic material like hematite. The magnetite amount, added components 2 and 3, is 37.5%; it has a $B_{1/2}$ of ~ 62 mT and a dispersion

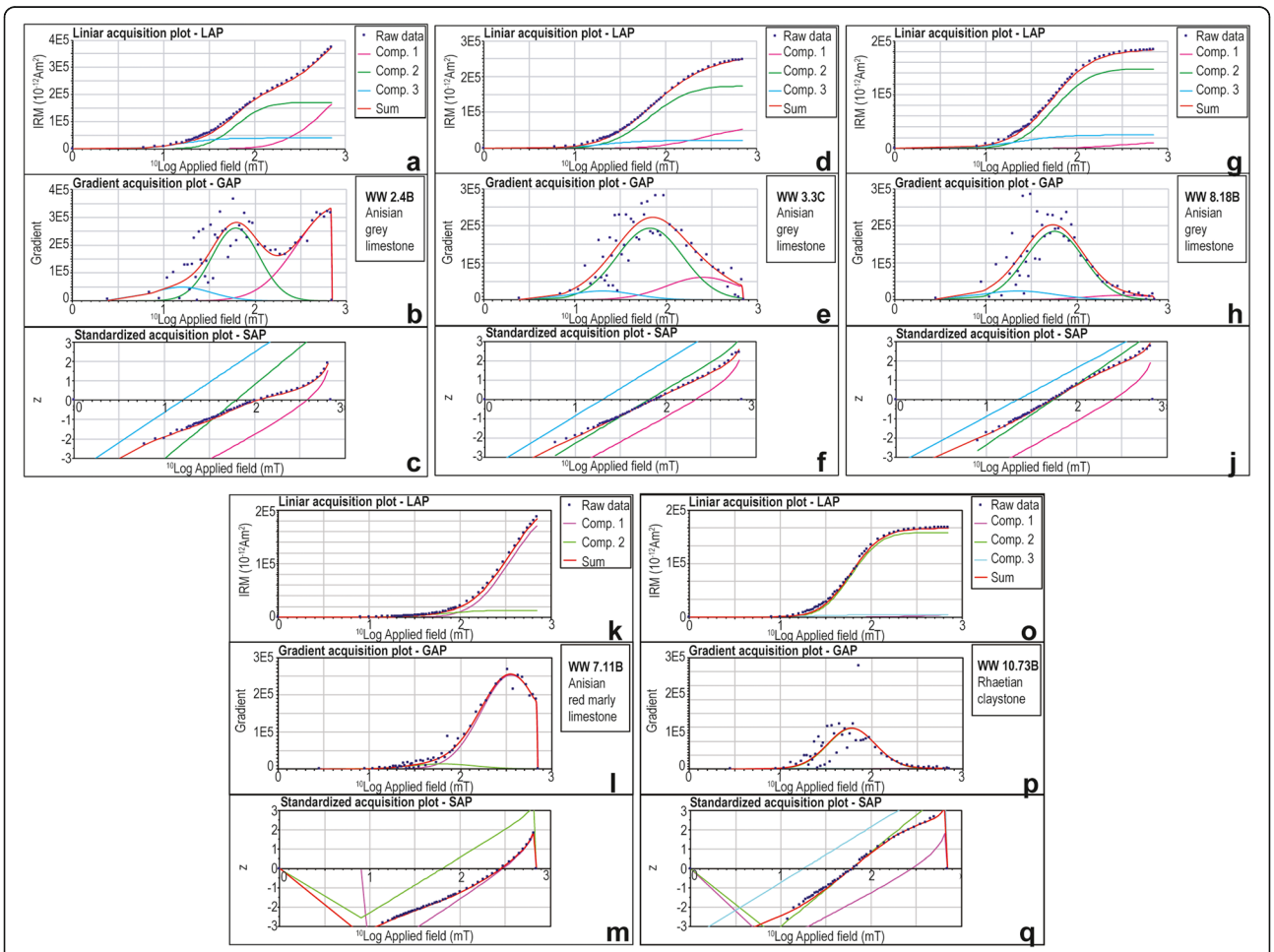

Fig. 3 Examples of coercivity component fits to IRM acquisition curves. **a-c** - Sample WW 2.4B from the Anisian grey limestone; **d-f** - Sample WW 3.3C from the Anisian grey limestone; **g, h, j** - Sample WW 8.18B from the Anisian grey limestone; **k-m** - Sample WW 7.11B from the Anisian red marly limestone; **o-q** - Sample WW 10.73B from the Rhaetian claystone. Component (Comp.) 1 (pink) is interpreted as hematite, Comp. 2 (green) is variably oxidized magnetite, and Comp. 3 (light blue) is the 'skew' component, see main text for detailed explanation. The sum of the components is marked in red; data points are the grey points. In the linear acquisition plots (LAP), i.e., **a, d, g, k, o**, the magnetic moment is plotted versus the logarithmic field value; in the gradient acquisition plots (GAP), i.e., **b, e, h, l, p**, the gradient of the LAP is plotted; in the standardized acquisition plots (SAP), i.e., **c, f, j, m, q**, the standardized score (z) is plotted versus the logarithmic field value. In this way of plotting deviations from cumulative log-Gaussian distributions show up as deviations from a straight line, indicating the need of additional components for a good fit

parameter of 0.26 which is in the often-observed range for relatively non-oxidized detrital magnetite (Kruiver et al. 2003). Magnetotactic magnetite would have a higher $B_{1/2}$ and a notably smaller DP, below 0.18 or even lower (e.g., Kruiver and Passier 2001; Egli 2004). The sample appears to have a reasonably low hematite amount; other samples show hematite amounts up to two orders of magnitude higher (Additional file 1: Supplementary Information 1b).

Sample WW 3.3C (Fig. 3) from the Anisian grey limestone contains 23.7% hematite with a lower $B_{1/2}$ of ~ 250 mT and a dispersion parameter of 0.4. When the relative amount of hematite decreases, it tends to be magnetically softer, hinting at a finer grain size. The magnetite (76.3%) is partially oxidized, in principle raising the $B_{1/2}$ value (here $B_{1/2}$ is ~ 66 mT) and the dispersion parameter value (0.36 in this sample). The dispersion parameter value is notably high for a ferrimagnetic material, indicating a broad switching field distribution which points at partially oxidized magnetite (Kruiver et al. 2003). Sample WW 8.18B from the Anisian grey limestone (Fig. 3) contains only 7% hematite with similar properties as in sample WW 3.3C. The dominant magnetite (93%) is fairly soft ($B_{1/2}$ ~ 56 mT) with a moderate dispersion parameter of 0.32. The thermally activated portion (component 3) seems to be higher in such samples.

Sample WW 7.11B also from the Anisian red marly limestone (Fig. 3) is evidently dominated by hematite with a hematite component representing almost 95% of the total IRM. It is relatively soft with the $B_{1/2}$ value being 355 mT and the dispersion parameter of 0.33. The minute amount of magnetite is probably oxidized with

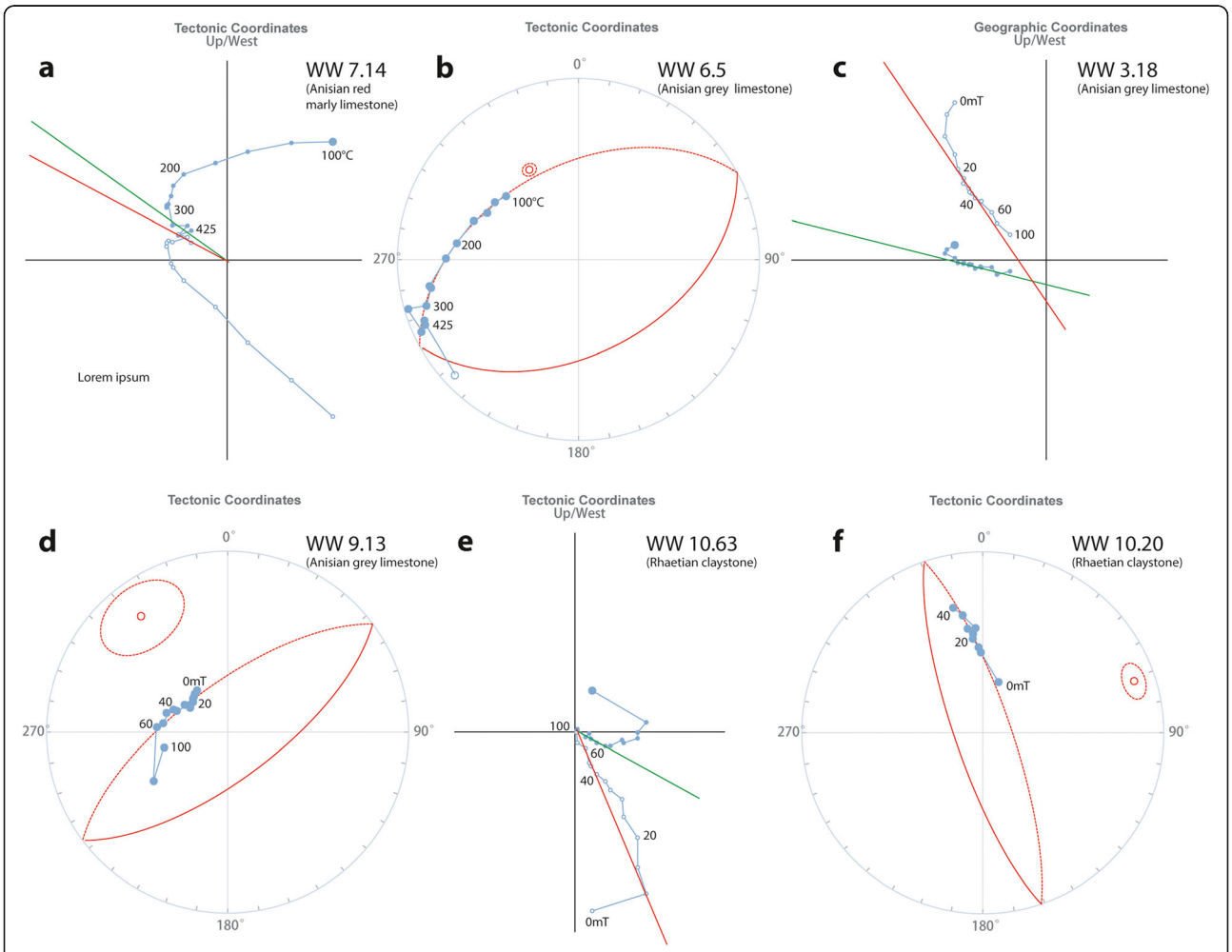

Fig. 4 Representative examples of orthogonal demagnetization diagrams (Zijderveld 1967) of the Anisian (WW 1–9) and Rhaetian (WW 10) samples from the Winterswijk quarry, both thermally (**a, b**) and by alternating fields (**c-f**). Characteristic Remanent Magnetizations (ChRM), called setpoints according to the terminology of McFadden and McElhinny (1988), could be determined occasionally (**a, c, e**). In the majority of the cases, however, the ChRM could not directly be determined and we calculated the best fitting plane (great circle) through the overprint and the origin (**b, d, f**)

its comparatively high $B_{1/2}$ of 63 mT and high dispersion parameter of 0.35.

Sample WW 10.73B from the Rhaetian claystone (Fig. 3) is magnetically dominated by magnetite (components 2 and 3 add up to 96.6%) with just about 3% as the hematite contribution. $B_{1/2}$ of magnetite is ~ 60 mT, together with the relatively low dispersion parameter (0.26), indicating non-oxidized magnetite. $B_{1/2}$ of hematite is ~ 400 mT, with the dispersion parameter of 0.42, indicating a broad grain size distribution.

Two groups of samples are distinguished: one with a low hematite content of < 40% (from a magnetic viewpoint) and another with a high hematite content of > 40% (Additional file 1: Supplementary Information 1a). The first group ($N = 44$) has an average of ~ 14% hematite, and the second group ($N = 8$) has an average of ~ 67% hematite. When the hematite amount is low, hematite appears to be magnetically softer: its average $B_{1/2}$ value is ~ 270 mT. In hematite-dominated samples, $B_{1/2}$ values are distinctly higher (average $B_{1/2}$ is ~ 610 mT). The magnetite in the low-hematite group is slightly softer as well with a $B_{1/2}$ of ~ 58 mT compared to ~ 61 mT for the high-hematite group. The standard deviations of both groups, however, largely overlap. Therefore, we recognize one type of magnetite throughout the studied section.

4.2 Demagnetization

4.2.1 Anisian

Both thermal and AF demagnetization of the Anisian samples (WW 1–9, see Additional files 1 and 2 for data files) show a large overprint of normal polarity with an approximately recent field (normal) direction which is likely due to the weathering of the rocks. It was not easily removed, and in only 10 samples we could determine a ChRM direction as a component which was of reversed polarity and decayed to the origin, so called setpoints (e.g., WW 7.14 from red marly limestone, Fig. 4a). The normal component dominates and the fully reversed direction that we find in the ChRM is not or not fully reached in all other samples. In that case, we determine a great circle (plane), fitting a selected arc of demagnetization data, assuming (1) there is no more than 2 components being simultaneously demagnetized in the arc, (2) the original component is contained in the plane but outside the selected demagnetization arc (e.g., WW 6.5 from grey limestone, Fig. 4b). AF demagnetization does not differ significantly from the thermal treatment, and we find both setpoints and great circles that are compatible with the thermal results (WW 3.18 and WW 9.13, both from grey limestones, Fig. 4c, d). We can now determine the mean directions (Table 1) either based on setpoints only (*sp*; $N = 13$) and/or based on combining setpoints and great circles (*sp* + *gc*; $N = 56$) using the iteration method to find the best-fit great circle solutions (McFadden and McElhinny 1988); the results of the two distributions are shown in Fig. 5. The means differ in declination (from $D_{sp} = 40.9 \pm 8.0°$ to $D_{sp+gc} = 30.8 \pm 3.0°$), and, not surprisingly, the error in declination (ΔD_x) becomes smaller with a larger number of samples in the two distributions. The difference in inclination (0.3°), however, is negligible (Table 1). Therefore, the test of the two means of sharing the same distribution using the bootstrap coordinate test (Tauxe 2010) is negative (Fig. 6).

4.2.2 Rhaetian

AF demagnetization of the Rhaetian samples (WW 10) shows a large overprint of normal polarity with an

Table 1 Palaeomagnetic data obtained from the Winterswijk quarry. Sites (site names) indicated with '(*sp*)' only include ChRM directions obtained by fitting linear segments of demagnetization paths (setpoints) interpreted using principal component analysis (Kirschvink 1980). Sites (site names) indicated with '(*sp* + *gc*)' also include great circle solutions referring to McFadden and McElhinny (1988)

Site Names	N_s	N_{45}	Dec		ΔD_x	Inc		ΔI_x	K	A_{95min}		A_{95}		A_{95max}	pLat	pLong	λ_{lo}		λ		λ_{hi}
Geographic Coordinates																					
Rhaetian (*sp*)	10	10	43.3	±	14.6	54.0	±	12.1	17.3	4.8	<	11.9	<	19.2	–	–	–		–		–
Rhaetian (*sp* + *gc*)	21	21	41.7	±	10.1	56.5	±	7.7	16.5	3.6	<	8.1	<	12.0	–	–	–		–		–
Anisian (*sp*)	13	13	224.5	±	8.4	−31.7	±	12.7	27.6	4.3	<	8.0	<	16.3	–	–	–		–		–
Anisian (*sp* + *gc*)	56	56	214.8	±	3.2	−31.3	±	4.9	39.4	2.4	<	3.1	<	6.5	–	–	–		–		–
Tectonic Coordinates																					
Rhaetian (*sp*)	10	10	34.2	±	12.6	48.7	±	12.6	20.5	4.8	<	10.9	<	19.2	56.9	123.4	20.0	<	29.7	<	42
Rhaetian (*sp* + *gc*)	21	21	32.0	±	8.7	50.9	±	8.1	19.3	3.6	<	7.4	<	12.0	60.6	123.9	24.8	<	31.6	<	39.8
Anisian (*sp*)	13	13	220.9	±	8.0	− 28.4	±	12.8	30.3	4.3	<	7.7	<	16.3	41.9	130.2	8.0	<	15.1	<	24
Anisian (*sp* + *gc*)	56	56	210.8	±	3.0	−26.7	±	4.9	43.9	2.4	<	2.9	<	6.5	45.0	142.0	11.3	<	14.1	<	17.1

Key to abbreviations: N_s = Number of interpreted ChRM directions; N_{45} = Number of directions after applying a 45° cutoff; Dec = Declination; ΔD_x (ΔI_x) = 95% confidence interval on the declination (inclination) following Butler (1992); Inc = Inclination; K = Fisher (1953) precision parameter calculated on virtual geomagnetic poles (VGPs); A_{95} = 95% cone of confidence around the VGPs; $A_{95(min,\ max)}$ = Reliability envelope of Deenen et al. (2011); pLat, pLong = Pole latitude and longitude; λ = Palaeolatitude; $\lambda_{(lo,\ hi)}$ = Lower and upper confidence limits for paleolatitude

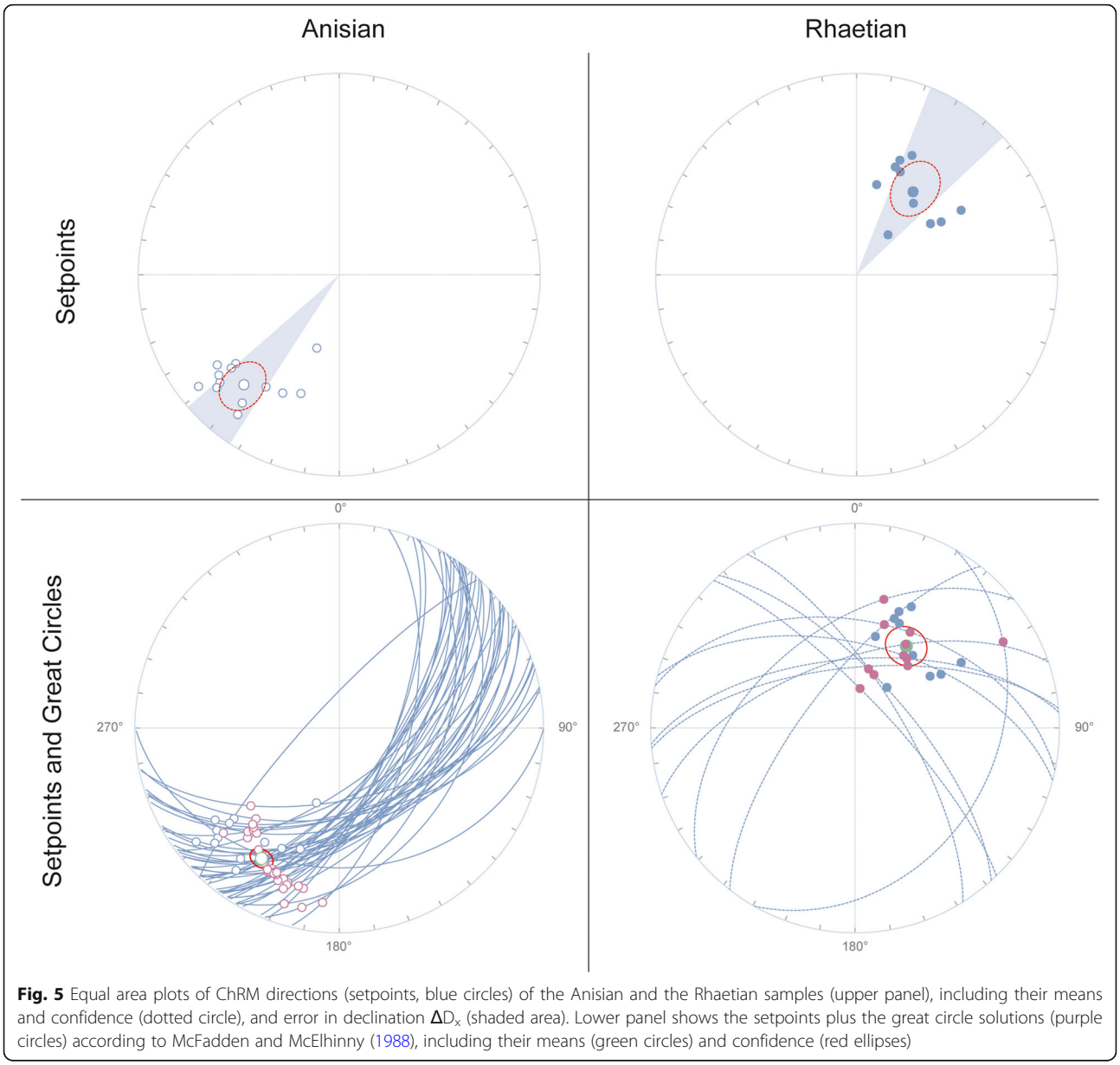

Fig. 5 Equal area plots of ChRM directions (setpoints, blue circles) of the Anisian and the Rhaetian samples (upper panel), including their means and confidence (dotted circle), and error in declination ΔD_x (shaded area). Lower panel shows the setpoints plus the great circle solutions (purple circles) according to McFadden and McElhinny (1988), including their means (green circles) and confidence (red ellipses)

approximately recent field (normal) direction. The overprint is also not easily removed and in only 10 samples we determine setpoints, of normal polarity, that decayed towards the origin (e.g., WW 10.63, Fig. 4e). In most cases, we could only determine a great circle (e.g., WW 10.20, Fig. 4f). We could only use AF demagnetization, so we cannot compare results with those from thermal treatment. We determine the mean directions (Table 1) based both on setpoints only (*sp*; $N = 10$) and on combining setpoints and great circle solutions ($sp + gc$; $N = 21$). The means of the two distributions do not differ significantly within error, neither in declination (from $D_{sp} = 34.2 \pm 12.6°$ to $D_{sp+gc} = 32.0 \pm 8.7°$) nor in inclination (differing by 0.1°; Table 1). In the case of the Rhaetian samples, the test of the two means of sharing the same distribution is positive (Tauxe 2010; Fig. 6), so the two means can be considered indistinguishable.

5 Discussion

5.1 Palaeomagnetic poles for the Anisian and the Rhaetian

The palaeomagnetic data for the Anisian and the Rhaetian as observed in the Triassic sediments from the Winterswijk quarry enable us to calculate the corresponding palaeomagnetic poles (Table 1), which we define as the mean of the VGP distributions with its

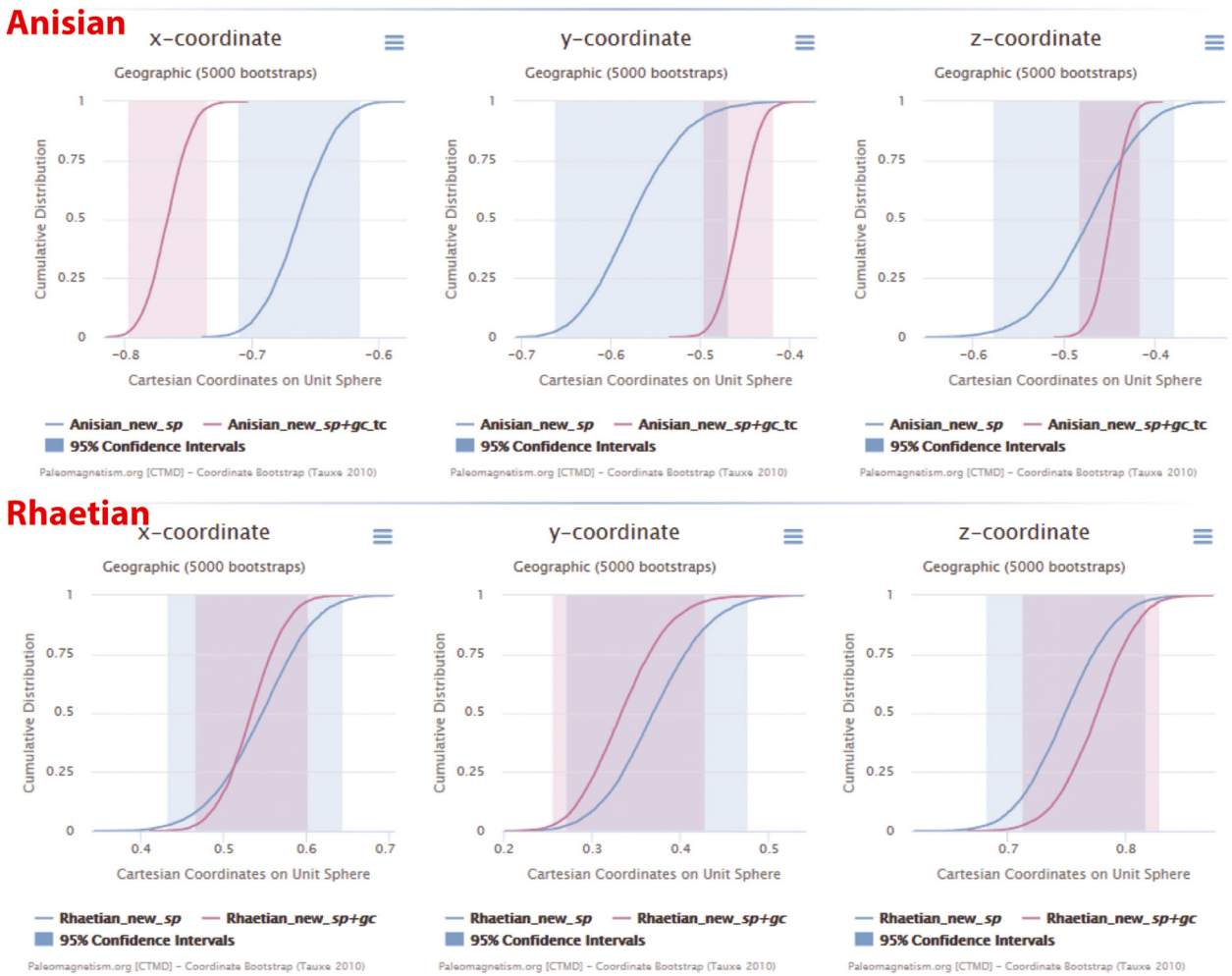

Fig. 6 Bootstrap Cartesian coordinate test (Tauxe 2010) showing that the distributions of setpoints (*sp*) versus setpoints+great circle solutions (*sp* + *gc*) of the Anisian do not share a common distribution, whereas the Rhaetian distributions share a common true mean direction. Coordinates are in a tectonic reference frame, and thus corrected for bedding tilt

corresponding K and A_{95}. The question is then which means — *sp* or *sp* + *gc* — we prefer. If we compare the two solutions for both the Anisian and the Raethian, we first note that the respective inclinations in both solutions are identical. The inclinations determine palaeolatitude and these are slightly lower but within an error of the predicted palaeolatitude for Eurasia according to the GAPWaP of Torsvik et al. (2012), which is based on 31 poles for the Anisian and 41 poles for the Rhaetian (Fig. 7). The Rhaetian palaeolatitude also conforms to the palaeolatitude predicted by the GAPWaP of Kent and Irving (2010), which does not continue back farther than 230 Ma and does not reach the Anisian (Fig. 7), and has a 210 Ma pole based on 11 palaeomagnetic poles. This further suggests that the Winterswijk sediments have faithfully recorded the field at the time of deposition, despite the pervasive overprint. We note that whilst for limestones such as those of the Muschelkalk, inclination shallows due to compaction is uncommon, fine clastics like those of the Rhaetian may have experienced some compaction-induced flattening. Given a large number of great circle solutions, we cannot apply common correction methods like the E/I method (e.g., Tauxe et al. 2008). Applying a commonly used flattening factor of 0.6 (e.g., Torsvik et al. 2012) would lead to a corrected inclination for the Rhaetian of ~ 45°, slightly higher than but still within an error of the GAPWaP of Torsvik et al. (2012).

In terms of declinations, however, there are some differences between the different solutions. For the Anisian, the declination from the *sp* + *gc* solution is close to the prediction for Eurasia by Kent and Irving (2010) and Torsvik et al. (2012) (Fig. 7) whereas from the *sp* solution the declination deviate by some 15° plots for the predicted declination curve, i.e., the observed *sp* declination is more

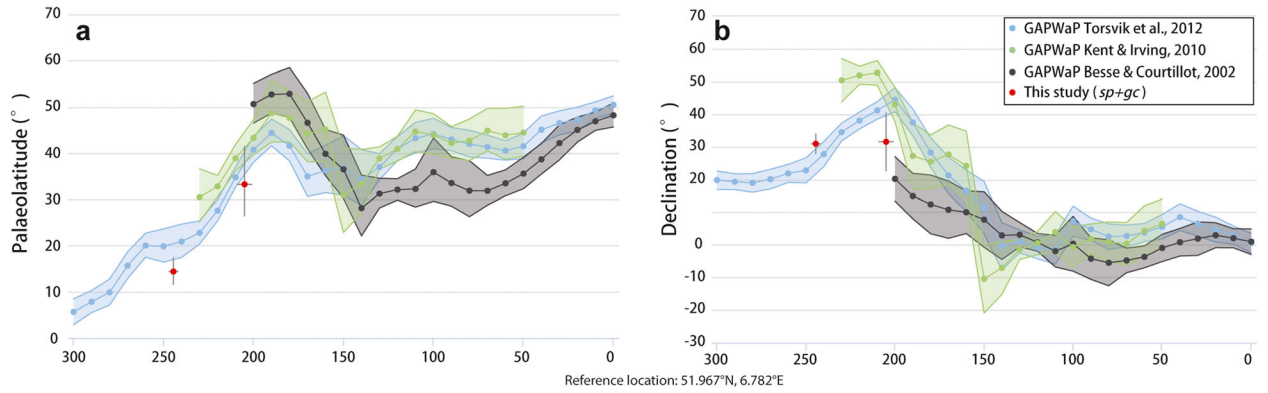

Fig. 7 **a** - Palaeolatitude and **b** - Declination versus time plots for sampling site illustrating predictions by different GAPWaPs, and by our new results

clockwise (~ 41 ± 8°) than expected (~ 26 ± 4°). For the Rhaetian, the *sp* solution has a declination (~ 34 ± 13°) that is close to the predicted declination (~ 43°), whereas the *sp* + *gc* solution (~ 32 ± 9°) is lower than expected by Kent and Irving (2010) and Torsvik et al. (2012), although in line with the trend predicted by the GAPWaP of Besse and Courtillot (2002) that stops at 200 Ma.

The question then arises which of our solutions provides the best option. We note that solutions with so many great circles are not ideal, and as a rule, we prefer to have more setpoints than great circle solutions so that possible biases in great circle solutions do not dominate. In the Winterswijk case, however, the great circles are very distinct and consistent, and we used only great circle interpretations of well-defined overprint components and a clear tendency towards the ChRM direction; components with noisy data in the Zijderveld diagrams were avoided. More importantly, the Rhaetian *sp* and *sp* + *gc* solutions share a common distribution and can be considered identical (Fig. 6). Hence, based on the consistent great circle solutions, the better fit of the Anisian *sp* + *gc* solution and the fact that the Rhaetian *sp* and *sp* + *gc* solutions are identical, we choose the *sp* + *gc* solutions as our best option to represent the Triassic poles of the Winterswijk sediments.

5.2 Triassic palaeogeography: position of the Netherlands in the heart of Pangea

Our new palaeomagnetic pole from the Anisian of Winterswijk corresponds well with the GAPWaP of Torsvik et al. (2012) (Fig. 8a). It is important to realize that a

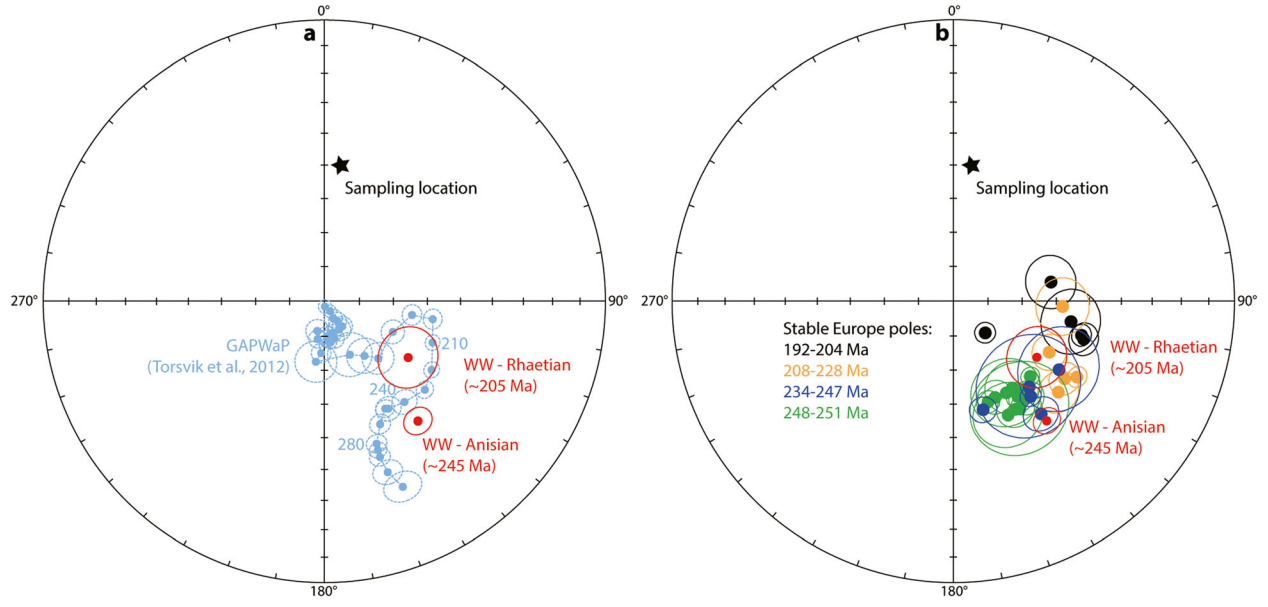

Fig. 8 Pole plots of the new Triassic poles from Winterswijk together with **a** - the GAPWaP of Torsvik et al. (2012); and, **b** - other Triassic stable Europe-derived poles used for the construction of the GAPWaP of Torsvik et al. (2012) (see their Table 1 for references and details)

GAPWaP is based on several tens of poles per time interval, and that the error bars shown for the GAPWaP result from averaging these poles. The actual scatter of the poles is considerably larger than the average 95% confidence limit of the GAPWaP, and our data points fall within that scatter as illustrated in Fig. 8b, where our new data fall within the cluster of contemporaneous poles from stable Eurasia. Figure 9 illustrates the palaeogeographic implication of these poles, showing the outline of the Netherlands within the supercontinent Pangea. This reconstruction follows Euler rotations for the major continents following Seton et al. (2012), with Neotethys and Paleotethys reconstructions following Muttoni et al. (2009), Gaina et al. (2013), Li et al. (2016) and Maffione and van Hinsbergen

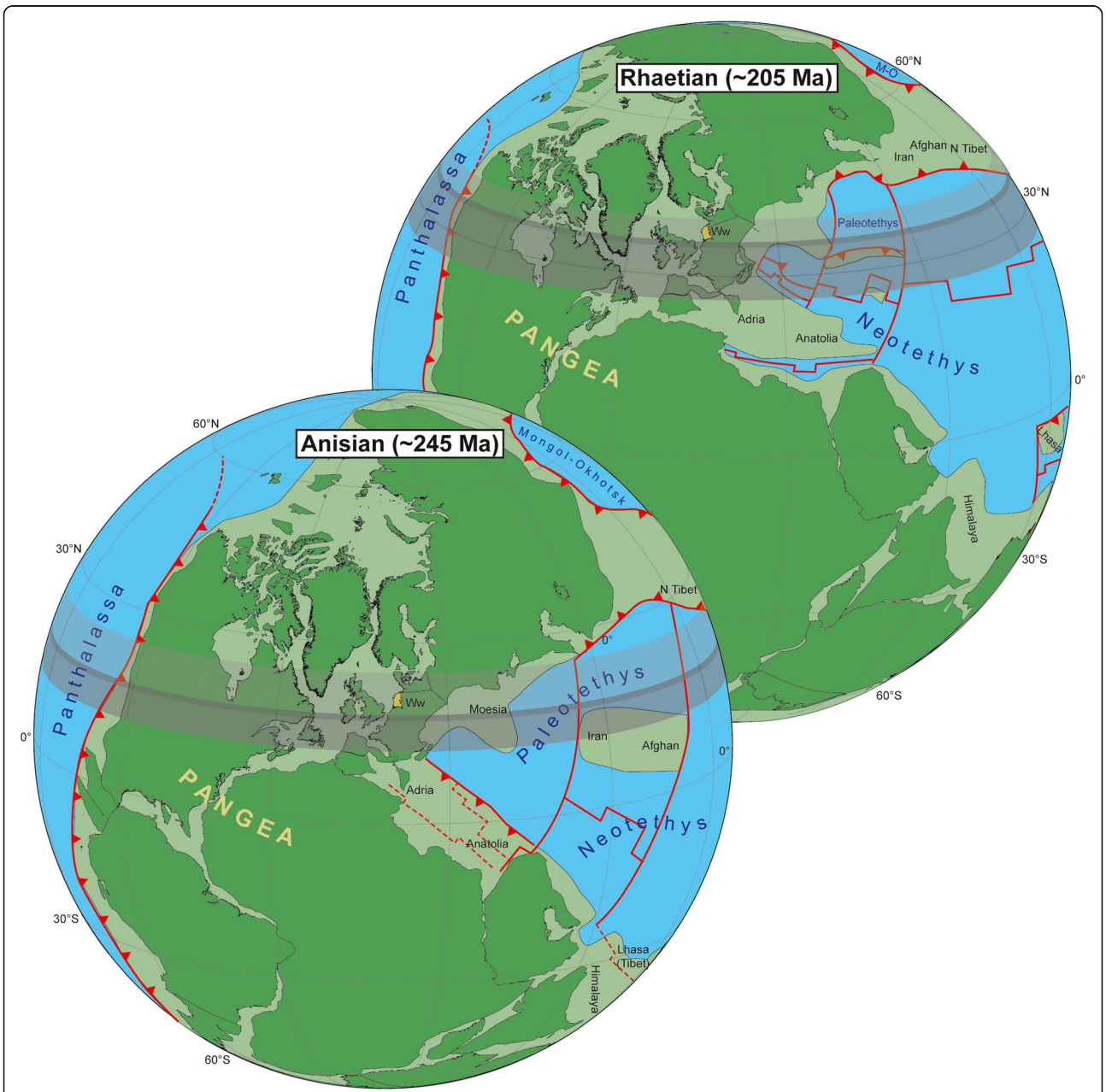

Fig. 9 Palaeogeographic maps of Pangea in the Anisian and the Rhaetian times, with the outline of the modern border of the Netherlands, and the sampling location in Winterswijk. Reconstructions based on Euler rotations of Seton et al. (2012) for the major continents, the Neotethys, and the Paleotethys based on Muttoni et al. (2009), Gaina et al. (2013), Li et al. (2016), Maffione and van Hinsbergen (2018), and East Asia following Van der Voo et al. (2015), cast in the palaeomagnetic reference frame of Torsvik et al. (2012). Light grey latitudinal band represents the palaeolatitude predicted by the GAPWaP, darker grey band is the palaeolatitude band predicted by our new Winterswijk poles, and the darkest grey thin band represents the overlap between the two palaeolatitude bands

(2018), and East Asia reconstruction following Van der Voo et al. (2015). The reconstruction is placed in the palaeomagnetic reference frame based on the GAPWaP of Torsvik et al. (2012), and illustrates the palaeolatitudes predicted by the Winterswijk sites.

Our new results further confirm that the Germanic Basin, with the large, epicontinental, shallow-marine Muschelkalk Sea, was located at low latitudes, at the Winterswijk locality ~ 15°N, within the heart of Pangea. This latitude corresponds to the modern Sahara Desert, providing an analogue for the environment in which the Buntsandstein Formation was deposited; and corresponds to the modern Persian Gulf that may be an analogy to the palaeogeographic setting of the Muschelkalk Basin, although the Muschelkalk Basin was in a post-collisional environment while the Persian Gulf was in a foreland of an ongoing collision. During the Rhaetian, in the early stages of Pangea breakup, the Germanic Basin had shifted to more northerly latitudes of ~ 30°N, corresponding to the modern latitude of e.g., Morocco and Sicily, causing the cooling trend on its way towards the modern latitude of 52°N (Table 1; Fig. 9).

6 Conclusions

We present two new Triassic palaeomagnetic poles for the stable Eurasian interior, based on the Anisian (247–242 Ma) blue-grey limestones and red marly limestones of the shallow-marine Muschelkalk Formation, and the Rhaetian (208–201 Ma) shallow-marine claystones exposed in a quarry at Winterswijk, the Netherlands. Rock magnetic experiments identify magnetite and hematite as carriers of the magnetization, depending on lithology. Demagnetization diagrams reveal a strong recent (GAD) overprint, as well as a second, low-inclination component at high coercivity and high unblocking temperature. This component is at times decaying towards the origin and is interpreted as the ChRM, whereas most specimens reveal great circles. Combining the great circle solutions with the isolated ChRMs, can lead to the two new palaeomagnetic poles that lie close to the predicted direction derived from GAPWaPs in Eurasian coordinates. Both poles may be included in future renditions of such paths, and confirm that the Germanic Basin, in which the Dutch Triassic was deposited, was located at an Anisian latitude around 14 ± 3°N, and was characterized by a palaeogeography similar to that of the Persian Gulf today. By the Rhaetian time, the basin was at 32 ± 7°N on its way to the modern latitude of 52°N.

7 Supplementary information

Supplementary information accompanies this paper at https://doi.org/10.1186/s42501-019-0046-2.

Additional file 1: Supplementary Information 1a Excel files of the IRM coercivity component fit for all samples. **Supplementary Information 1b** An overview of the input data for the IRM-CGL1.0 excel workbook (Kruiver et al. 2001).

Additional file 2: Demagnetization data (.dir files) and interpreted directions for statistical analysis (.pmag file) for the Winterswijk locality, compatible with the Paleomagnetism.org online analysis software. WW 1–9 samples refer to the Anisian (Anisian_pole.dir) whereby WW 1, 5, 6, 7 are from red marly limestones, and WW 2, 3, 4, 8, 9 are from grey limestones; WW 10 samples refer to the Rhaetian (Rhaetian_pole.dir).

Abbreviations

°N: Degrees North (latitude); A_{95}: 95% cone of confidence around the virtual geomagnetic poles; AF: Alternating field; ARM: Anhysteretic remanent magnetization; ChRM: Characteristic remanent magnetization; D: Declination; DP: Dispersion parameter; GAD: Geocentric axial dipole; GAP: Gradient acquisition plots; GAPWaP: Global apparent polar wander path; *gc*: Great circle; I: Inclination; IRM: Isothermal remanent magnetization; K (k or κ): Fisher (1953) precision parameter calculated on virtual geomagnetic poles; LAP: Linear acquisition plots; Lat: Latitude; Lon: Longitude; MAD: Maximum angular deviation; NRM: Natural remanent magnetization; nT, mT, T: nano-Tesla, milli-Tesla, Tesla; SAP: Standardized acquisition plots; SIRM: Saturation isothermal remanent magnetization; *sp*: Set point; VGP: Virtual geomagnetic pole; ΔD_x: Declination error; ΔI_x: Inclination error

Acknowledgements

We thank Flora Boekhout for participating in sampling. We appreciated the help and introduction in the geology of the Winterswijk quarry for the 2007 sampling trip by the late Henk Oosterink, who has done excellent and extensive work on the geology and palaeontology of the Dutch Triassic. We thank Vicente-Carlos Ruiz-Martinez and an anonymous reviewer for their helpful comments.

Authors' contributions

LPPvH conceived of the study, performed sampling, and carried out palaeomagnetic laboratory analyses. DJJvH conceived of the study, performed sampling, analyzed data, and drafted the manuscript. CGL and MJD analyzed data and drafted the manuscript. BZ carried out palaeomagnetic laboratory analyses. MHLD performed sampling and carried out palaeomagnetic laboratory analyses. All authors read and approved the final manuscript.

Funding

Douwe J.J. van Hinsbergen was funded through NWO Vidi Grant 864.11.004 and NWO Vici Grant 865.17.001.

Availability of data and materials

All demagnetization diagrams, interpreted palaeomagnetic components, and statistical files are available in the Additional files 1 and 2 and can be uploaded, viewed, and edited on Paleomagnetism.org (Koymans et al. 2016). Rock magnetic data files are available in the Additional files 1 and 2.

Competing interests

The authors declare that they have no competing interests.

Author details

[1]Fioretti College, Sportlaan 3, 2161 VA Lisse, the Netherlands. [2]Department of Earth Sciences, Utrecht University, Princetonlaan 8A, 3584 CB Utrecht, the Netherlands. [3]Twents Carmel College De Thij, Thijlaan 30, 7576 ZB Oldenzaal, the Netherlands.

Received: 2 October 2018 Accepted: 1 October 2019
Published online: 08 November 2019

References

Albat, F. 1999. Tetrapod footprints in the lower Muschelkalk of Borgholzhausen — A field report. *Geologie und Paläontologie in Westfalen* 52: 19–39.

Albers, P. 2011. New Nothosaurus skulls from the lower Muschelkalk of the western Lower Saxony Basin (Winterswijk, the Netherlands) shed new

light on the status of Nothosaurus winterswijkensis. *Netherlands Journal of Geosciences* 90: 15–22.

Baatsen, M., D.J.J. van Hinsbergen, A.S. von der Heydt, H.A. Dijkstra, A. Sluijs, H.A. Abels, and P.K. Bijl. 2016. Reconstructing geographical boundary conditions for palaeoclimate modelling during the Cenozoic. *Climate of the Past* 12: 1635–1644.

Besse, J., and V. Courtillot. 2002. Apparent and true polar wander and the geometry of the geomagnetic field over the last 200 Myr. Journal of Geophysical Research - Solid Earth 107: EPM 6–1-31.

Bickelmann, C., and P.M. Sander. 2008. A partial skeleton and isolated humeri of Nothosaurus (Reptilia: Eosauropterygia) from Winterswijk, the Netherlands. *Journal of Vertebrate Paleontology* 28: 326–338.

Blakey, R.C. 2008. Gondwana paleogeography from assembly to breakup — A 500 m.y. odyssey. In: Fielding, C.R., T.D. Frank and J.L. Isbell. (Eds.). Resolving the late Paleozoic ice age in time and space. Geological Society of America special paper 441: 521–529.

Boschman, L.M., D.J.J. van Hinsbergen, T.H. Torsvik, W. Spakman, and J.L. Pindell. 2014. Kinematic reconstruction of the Caribbean region since the early Jurassic. *Earth-Science Reviews* 138: 102–136.

Butler, R.F. 1992. *Paleomagnetism: Magnetic domains to geologic Terranes*. Boston: Blackwell Scientific Publications.

Cogné, J.-P., J. Besse, Y. Chen, and F. Hankard. 2013. A new late cretaceous to present APWP for Asia and its implications for paleomagnetic shallow inclinations in Central Asia and Cenozoic Eurasian plate deformation. *Geophysical Journal International* 192: 1000–1024.

Cox, A., and R.B. Hart. 1986. Plate tectonics: How it works. John Wiley & Sons.

Deenen, M.H.L., C.G. Langereis, D.J.J. van Hinsbergen, and A.J. Biggin. 2011. Geomagnetic secular variation and the statistics of palaeomagnetic directions. *Geophysical Journal International* 186: 509–520.

Deenen, M.H.L., C.G. Langereis, D.J.J. van Hinsbergen, and A.J. Biggin. 2014. Erratum: Geomagnetic secular variation and the statistics of palaeomagnetic directions. *Geophysical Journal International* 197: 643–643.

Demathieu, G., and H. Oosterink. 1988. New discoveries of ichnofossils from the middle Triassic of Winterswijk (the Netherlands). *Geologie en Mijnbouw* 67: 3–17.

Diedrich, C. 2000. New vertebrate tracks from the lower Muschelkalk (middle Triassic) of the Osnabrueck Hills and Teutoburg Forest (NW-Germany) and their stratigraphic and palaeogeographic significance in the Germanic Basin. *Neues Jahrbuch für Geologie und Paläontologie Abhandlungen* 217: 369–395.

Dupont-Nivet, G., D.J.J. van Hinsbergen, and T.H. Torsvik. 2010. Persistently low Asian paleolatitudes: Implications for the India-Asia collision history. *Tectonics* 29. https://doi.org/10.1029/2008tc002437.

During, M., D. Voeten, A. Schulp, and J. Reumer. 2017. A possible Pararcus diepenbroeki vertebra from the Vossenveld formation (Triassic, Anisian), Winterswijk, the Netherlands. *Netherlands Journal of Geosciences* 96: 63–68.

Egli, R. 2004. Characterization of individual rock magnetic components by analysis of remanence curves, 1. Unmixing natural sediments. *Studia Geophysica et Geodaetica* 48: 391–446.

Fisher, R. 1953. Dispersion on a sphere. *Proceedings of the Royal Society of London. Series A: Mathematical and Physical Sciences* 217: 295–305.

Gaina, C., T.H. Torsvik, D.J.J. van Hinsbergen, S. Medvedev, S.C. Werner, and C. Labails. 2013. The African plate: A history of oceanic crust accretion and subduction since the Jurassic. *Tectonophysics* 604: 4–25.

Gradstein, F.M., J.G. Ogg, M. Schmitz, and G. Ogg. 2012. The geologic time scale 2012. Elsevier.

Hall, R. 2002. Cenozoic geological and plate tectonic evolution of SE Asia and the SW Pacific: Computer-based reconstructions, model and animations. *Journal of Asian Earth Sciences* 20: 353–431.

Heijne, J., N. Klein, and P.M. Sander. 2019. The uniquely diverse taphonomy of the marine reptile skeletons (Sauropterygia) from the lower Muschelkalk (Anisian) of Winterswijk, the Netherlands. *Paläontologische Zeitschrift* 93: 69–92.

Herngreen, G., J. Van Konijnenburg-van Cittert, and H. Oosterink. 2005. New geological data (middle Triassic, Rhaetian-Liassic and Oligocene) of the Winterswijk quarry, the eastern Netherlands. *Netherlands Journal of Geosciences* 84: 409–413.

Heslop, D., G. McIntosh, and M. Dekkers. 2004. Using time-and temperature-dependent Preisach models to investigate the limitations of modelling isothermal remanent magnetization acquisition curves with cumulative log Gaussian functions. *Geophysical Journal International* 157: 55–63.

Kent, D.V., and E. Irving. 2010. Influence of inclination error in sedimentary rocks on the Triassic and Jurassic apparent pole wander path for North America and implications for cordilleran tectonics. *Journal of Geophysical Research* 115: B10103. https://doi.org/10.1029/2009JB007205.

Kirschvink, J. 1980. The least-squares line and plane and the analysis of palaeomagnetic data. *Geophysical Journal International* 62: 699–718.

Klein, N. 2009. Skull morphology of Anarosaurus heterodontus (Reptilia: Sauropterygia: Pachypleurosauria) from the lower Muschelkalk of the Germanic Basin (Winterswijk, the Netherlands). *Journal of Vertebrate Paleontology* 29: 665–676.

Klein, N. 2012. Postcranial morphology and growth of the pachypleurosaur Anarosaurus heterodontus (Sauropterygia) from the lower Muschelkalk of Winterswijk, the Netherlands. *Paläontologische Zeitschrift* 86: 389–408.

Klein, N., and P.C. Albers. 2009. A new species of the sauropsid reptile Nothosaurus from the lower Muschelkalk of the western Germanic Basin, Winterswijk, the Netherlands. *Acta Palaeontologica Polonica* 54: 589–598.

Klein, N., and E.M. Griebeler. 2018. Growth patterns, sexual dimorphism, and maturation modeled in Pachypleurosauria from middle Triassic of Central Europe (Diapsida: Sauropterygia). *Fossil Record* 21: 137–157.

Klein, N., and T.M. Scheyer. 2013. A new placodont sauropterygian from the middle Triassic of the Netherlands. *Acta Palaeontologica Polonica* 59: 887–902.

Klein, N., and O.J. Sichelschmidt. 2014. Remarkable dorsal ribs with distinct uncinate processes from the early Anisian of the Germanic Basin (Winterswijk, the Netherlands). *Neues Jahrbuch für Geologie und Paläontologie Abhandlungen* 271: 307–314.

Klein, N., D.F. Voeten, A. Haarhuis, and R. Bleeker. 2016. The earliest record of the genus Lariosaurus from the early middle Anisian (middle Triassic) of the Germanic Basin. *Journal of Vertebrate Paleontology* 36: e1163712.

Klein, N., D.F. Voeten, J. Lankamp, R. Bleeker, O.J. Sichelschmidt, M. Liebrand, D.C. Nieweg, and P.M. Sander. 2015. Postcranial material of Nothosaurus marchicus from the lower Muschelkalk (Anisian) of Winterswijk, the Netherlands, with remarks on swimming styles and taphonomy. *Paläontologische Zeitschrift* 89: 961–981.

Klompmaker, A., and B. Van den Berkmortel. 2007. Earliest Jurassic (Hettangian) psiloceratoid ammonites from a subrosion pipe at Winterswijk, the eastern Netherlands. *Netherlands Journal of Geosciences-Geologie en Mijnbouw* 86: 379.

Klompmaker, A.A., and R.H. Fraaije. 2011. The oldest (middle Triassic, Anisian) lobsters from the Netherlands: Taxonomy, taphonomy, paleoenvironment, and paleoecology. *Palaeontologia Electronica* 14: 1–16.

Klompmaker, A.A., G.W. Herngreen, and H.W. Oosterink. 2010. Biostratigraphic correlation, paleoenvironment stress, and subrosion pipe collapse: Dutch Rhaetian shales uncover their secrets. *Facies* 56: 597–613.

Kloprogge, J.T., H. Ruan, L.V. Duong, and R.L. Frost. 2001. FT-IR and Raman microscopic study at 293 K and 77 K of celestine, $SrSO_4$, from the middle triassic limestone (Muschelkalk) in Winterswijk, the Netherlands. *Netherlands Journal of Geosciences* 80: 41–47.

Koymans, M.R., C.G. Langereis, D. Pastor-Galán, and D.J.J. van Hinsbergen. 2016. Paleomagnetism.org: An online multi-platform open source environment for paleomagnetic data analysis. *Computers & Geosciences* 93: 127–137.

Kruiver, P.P., M.J. Dekkers, and D. Heslop. 2001. Quantification of magnetic coercivity components by the analysis of acquisition curves of isothermal remanent magnetisation. *Earth and Planetary Science Letters* 189: 269–276.

Kruiver, P.P., C.G. Langereis, M.J. Dekkers, and W. Krijgsman. 2003. Rock-magnetic properties of multicomponent natural remanent magnetization in alluvial red beds (NE Spain). *Geophysical Journal International* 153: 317–332.

Kruiver, P.P., and H.F. Passier. 2001. Coercivity analysis of magnetic phases in sapropel S1 related to variations in redox conditions, including an investigation of the S ratio. *Geochemistry, Geophysics, Geosystems* 2 (12): 1063. https://doi.org/10.1029/2001GC000181.

Li, S., E.L. Advokaat, D.J.J. van Hinsbergen, M. Koymans, C. Deng, and R. Zhu. 2017. Paleomagnetic constraints on the Mesozoic-Cenozoic paleolatitudinal and rotational history of Indochina and South China: Review and updated kinematic reconstruction. *Earth-Science Reviews* 171: 58–77.

Li, Z., L. Ding, P.C. Lippert, P. Song, Y. Yue, and D.J.J. van Hinsbergen. 2016. Paleomagnetic constraints on the Mesozoic drift of the Lhasa Terrane (Tibet) from Gondwana to Eurasia. *Geology* 44: 727–730.

Maffione, M., and D.J.J. van Hinsbergen. 2018. Reconstructing plate boundaries in the Jurassic neo-Tethys from the east and west Vardar Ophiolites (Greece, Serbia). *Tectonics* 37: 858–887.

Maxwell, E.E., H. Diependaal, H. Winkelhorst, G. Goris, and N. Klein. 2016. A new species of Saurichthys (Actinopterygii: Saurichthyidae) from the middle Triassic of Winterswijk, the Netherlands. *Neues Jahrbuch für Geologie und Paläontologie Abhandlungen* 280: 119–134.

McFadden, P., and M. McElhinny. 1988. The combined analysis of remagnetization circles and direct observations in palaeomagnetism. *Earth and Planetary Science Letters* 87: 161–172.

Mullender, T.A.T., T. Frederichs, C. Hilgenfeldt, L.V. de Groot, K. Fabian, and M.J. Dekkers. 2016. Automated paleomagnetic and rock magnetic data acquisition with an in-line horizontal "2G" system. *Geochemistry, Geophysics, Geosystems* 17: 3546–3559.

Mullender, T.A.T., A.J. Van Velzen, and M.J. Dekkers. 1993. Continuous drift correction and separate identification of ferrimagnetic and paramagnetic contributions in thermomagnetic runs. *Geophysical Journal International* 114: 663–672.

Muttoni, G., M. Mattei, M. Balini, A. Zanchi, M. Gaetani, and F. Berra. 2009. The drift history of Iran from the Ordovician to the Triassic. *Geological Society, London, Special Publications* 312: 7–29.

Nokleberg, W.J., L.M. Parfenov, J.W.H. Monger, I.O. Norton, A. Khanchuk, D.B. Stone, C.R. Scotese, D.W. Scholl, and K. Fujita. 2000. Phanerozoic tectonic evolution of the Circum-North Pacific. U.S. Department of the Interior. U.S. Geological Survey.

Oosterink, H. 1976. Fossiele voetstappen in de eerste Muschelkalk-groeve van Winterswijk. *Grondboor & Hamer* 30: 130–144.

Oosterink, H., T. Simon, H. Hagdorn, and H. Winkelhorst. 2006. A subrosion pipe fill in the lower Muschelkalk, Winterswijk quarry, eastern Netherlands. *Netherlands Journal of Geosciences* 85: 293–297.

Passier, H., G. De Lange, and M. Dekkers. 2001. Magnetic properties and geochemistry of the active oxidation front and the youngest sapropel in the eastern Mediterranean Sea. *Geophysical Journal International* 145: 604–614.

Sander, P.M., N. Klein, P.C. Albers, C. Bickelmann, and H. Winkelhorst. 2014. Postcranial morphology of a basal Pistosauroidea (Sauropterygia) from the lower Muschelkalk of Winterswijk, the Netherlands. *Paläontologische Zeitschrift* 88: 55–71.

Schulp, A.S., R.W. Bleeker, A. Haarhuis, E. van Spronsen, M.A. During, G. Goris, P. Kaskes, Y. Matteman, W. Winkelhorst, and H. Winkelhorst. 2017. A tetrapod swimming traceway from the Triassic of Winterswijk, the Netherlands. *Netherlands Journal of Geosciences* 96: 273–277.

Scotese, C., and A. Schettino. 2017. Late Permian-early Jurassic paleogeography of Western Tethys and the world, Permo-Triassic salt provinces of Europe, North Africa and the Atlantic margins. Elsevier, pp. 57–95.

Seton, M., R.D. Müller, S. Zahirovic, C. Gaina, T. Torsvik, G. Shephard, A. Talsma, M. Gurnis, M. Turner, S. Maus, and M. Chandler. 2012. Global continental and ocean basin reconstructions since 200 ma. *Earth-Science Reviews* 113: 212–270.

Sier, M.J., W. Roebroeks, C.C. Bakels, M.J. Dekkers, E. Bruhl, D. De Loecker, S. Gaudzinski-Windheuser, N. Hesse, A. Jagich, L. Kindler, W.J. Kuijper, T. Laurat, H.J. Mucher, K.E. Penkman, D. Richter, and D.J.J. van Hinsbergen. 2011. Direct terrestrial-marine correlation demonstrates surprisingly late onset of the last interglacial in Central Europe. *Quaternary Research* 75: 213–218.

Tauxe, L. 2010. Essentials of Paleomagnetism. University of California Press.

Tauxe, L., K.P. Kodama, and D.V. Kent. 2008. Testing corrections for paleomagnetic inclination error in sedimentary rocks: A comparative approach. *Physics of the Earth and Planetary Interiors* 169: 152–165.

Torsvik, T.H., and L.R.M. Cocks. 2017. Earth history and Palaeogeography. Cambridge University Press.

Torsvik, T.H., R.D. Müller, R. Van der Voo, B. Steinberger, and C. Gaina. 2008. Global plate motion frames: Toward a unified model. *Reviews of Geophysics*: 46. https://doi.org/10.1029/2007rg000227.

Torsvik, T.H., R. Van der Voo, U. Preeden, C. Mac Niocaill, B. Steinberger, P.V. Doubrovine, D.J.J. van Hinsbergen, M. Domeier, C. Gaina, E. Tohver, J.G. Meert, P.J.A. McCausland, and L.R.M. Cocks. 2012. Phanerozoic polar wander, palaeogeography and dynamics. *Earth-Science Reviews* 114: 325–368.

Van der Voo, R., D.J.J. van Hinsbergen, M. Domeier, W. Spakman, and T.H. Torsvik. 2015. Latest Jurassic–earliest cretaceous closure of the Mongol-Okhotsk Ocean: A paleomagnetic and seismological-tomographic analysis. *Geological Society of America, Special Paper* 513: 589–606. https://doi.org/10.1130/2015.2513(19).

van Eldijk, T., G. Goris, A. Haarhuis, J. Lankamp, H. Winkelhorst, J. Reumer, A. Nel, and T. Wappler. 2017. New fossil insects from the Anisian (lower to middle Muschelkalk) from the central European Basin (Germany and the Netherlands). *Paläontologische Zeitschrift* 91: 185–194.

van Hinsbergen, D.J.J., L.V. de Groot, S.J. van Schaik, W. Spakman, P.K. Bijl, A. Sluijs, C.G. Langereis, and H. Brinkhuis. 2015. A paleolatitude calculator for paleoclimate studies. *PLoS One* 10: e0126946.

van Hinsbergen, D.J.J., P.C. Lippert, S. Li, W. Huang, E.L. Advokaat, and W. Spakman. 2019. Reconstructing greater India: Paleogeographic, kinematic, and geodynamic perspectives. *Tectonophysics* 760: 69–94.

van Hinsbergen, D.J.J., R.L. Vissers, and W. Spakman. 2014. Origin and consequences of western Mediterranean subduction, rollback, and slab segmentation. *Tectonics* 33: 393–419.

Vérard, C., C. Hochard, P.O. Baumgartner, and G.M. Stampfli. 2015. Geodynamic evolution of the earth over the Phanerozoic: Plate tectonic activity and palaeoclimatic indicators. *Journal of Palaeogeography* 4: 167–188.

Voeten, D.F., T. Reich, R. Araújo, and T.M. Scheyer. 2018. Synchrotron microtomography of a Nothosaurus marchicus skull informs on nothosaurian physiology and neurosensory adaptations in early Sauropterygia. *PLoS One* 13: e0188509.

Voeten, D.F., P.M. Sander, and N. Klein. 2015. Skeletal material from larger Eusauropterygia (Reptilia: Eosauropterygia) with nothosaurian and cymatosaurian affinities from the lower Muschelkalk of Winterswijk, the Netherlands. *Paläontologische Zeitschrift* 89: 943–960.

Ziegler, P. 1992. North Sea rift system. *Tectonophysics* 208: 55–75.

Zijderveld, J.D.A. 1967. A. C. Demagnetization of Rocks: Analysis of Results. In: Developments in Solid Earth Geophysics, Volume 3, Elsevier, pp. 254–286.

Publisher's Note